# Formic acid catalyzed keto-enol tautomerizations for C2 and C3 enols: Implications in atmospheric and combustion chemistry

# Formic acid catalyzed keto-enol tautomerizations for $C_2$ and $C_3$ enols. Implications in atmospheric and combustion chemistry

Manuel Monge-Palacios,[1] Edwing Grajales-González[1] and Subram Mani Sarathy[1]

## Abstract

Enols are important species in atmospheric and combustion chemistry. However, their implications in these systems are not well established due to a lack of accurate rate constants and mechanisms to determine their fate. In this work, we investigate the formic acid catalyzed keto–enol tautomerizations converting vinyl alcohol, propen-2-ol and 1-propenol into acetaldehyde, acetone and propanal, respectively. High-level *ab initio* and multi-structural torsional variational transition state theory calculations are performed with small-curvature tunnelling corrections to obtain rate constants in the temperature range 200–3000 K. Tunnelling is shown to be pronounced as a consequence of very narrow adiabatic potential energy curves, and indicates a need to revisit previous calculations. We show the implications of the studied reactions on the fate of enols under combustion relevant conditions by detailed kinetic modelling simulations. The yield of vinyl alcohol predicted by our calculated rate constants may be useful to lessen the underestimation of organic acids concentrations in current atmospheric models.

## KEYWORDS

Ab initio, rate constants, keto-enol tautomerizations, combustion chemistry, atmospheric chemistry.

---

[1]King Abdullah University of Science and Technology (KAUST), Clean Combustion Research Center (CCRC), Physical Science and Engineering (PSE), Thuwal 23955-6900, Saudi Arabia.

**Corresponding author**

Manuel Monge-Palacios

Email: mongepalaciosm@gmail.com

**Funding information**

King Abdullah University of Science and Technology (KAUST), Office of Sponsored Research (OSR), Award No. OSR-2016-CRG5-3022

## 1. INTRODUCTION

Enols are important species in many combustion systems,[1] but they are usually absent in kinetic models for hydrocarbon oxidation. Keto–enol tautomerizations are important intermediate steps in the production of carboxylic acids in the troposphere and may shed light into the carboxylic acids atmospheric budget, which is underestimated by current kinetic models.[2,3] Andrews *et al*.[2] and Shaw *et al*.[3] determined that photo-tautomerization of acetaldehyde ($CH_3CHO$) forming vinyl alcohol ($CH_2CHOH$) contributes to the yield of tropospheric formic acid (HCOOH), which can be produced by the oxidation of $CH_2CHOH$. These studies suggest that some sources of carboxylic acids might be missing or underestimated, and highlight the need for a better understanding of enol chemistry in order to quantify their fate in atmospheric and combustion systems.

Larger enols (i.e., larger than vinyl alcohol), whose chemistry is not well stablished, can be also produced via tautomerization of corresponding carbonyls, and subsequently oxidized to produce larger carboxylic acids, which may help to explain the observed discrepancies between modelling and measurements. This is the case of the keto–enol tautomerizations of propen-2-ol (i-$C_3H_5OH$) and 1-propenol ($CH_3CHCHOH$) into acetone ($CH_3COCH_3$) and propanal ($CH_3CH_2CHO$), respectively. The unimolecular gas-phase tautomerization of enols to aldehydes/ketones has a high barrier height,[4] but these reactions can be catalyzed by HCOOH.[5,6] These HCOOH-catalyzed reactions proceed via a double hydrogen shift mechanism:

$$\text{i-}C_3H_5OH + HCOOH \Leftrightarrow CH_3COCH_3 + HCOOH \quad \text{(R1)}$$

$$CH_3CHCHOH + HCOOH \Leftrightarrow CH_3CH_2CHO + HCOOH \quad \text{(R2)}$$

$$CH_2CHOH + HCOOH \Leftrightarrow CH_3CHO + HCOOH \quad \text{(R3)}$$

Due to the lack of information on R1 and R2, recent studies on the combustion of butanol isomers[4,7,8] have used the rate constants calculated by da Silva[5] for R3 as an analogy.

The kinetics of the reaction R3 was revisited by Peeters *et al*.,[6] and their rate constants in the limited temperature range 280–320 K are around 5 orders of magnitude lower than those reported by da Silva.[5] Peeters used the CBS-UCCSD(T)//UQCISD/6-311++G(d,p) level and transition state theory for the calculations, while da Silva used the lower composite level G3SX[9] and the master equation approach. Both used the Eckart approach to estimate tunneling, which does not consider the curvature of the reaction path and may not be accurate. This overestimation of the

rate constants for R3 by da Silva may overestimate the role of reactions R1, R2 and R3 in combustion[7] and atmospheric modeling.

Accurate rate constants for the reactions R1, R2 and R3 are crucial for developing kinetic models that investigate the fate of the involved species in the atmosphere, as well as the combustion of biofuels like ethanol and butanol.[10] Therefore, this work performs a kinetic study of the reactions R1, R2, and R3 across a wide temperature range which is of interest in combustion and atmospheric chemistry. This allows us to derive some conclusions about the reactivity of three different enols, i-$C_3H_5OH$, $CH_3CHCHOH$ and $CH_2CHOH$, towards HCOOH, shed light into their implications in atmospheric and combustion chemistry, and formulate new and more accurate analogue reactions for kinetic modeling of larger enols and aldehydes/ketones.

## 2. METHODS AND COMPUTATIONAL DETAILS

Multi-structural torsional variational transition state theory with a coupled torsional potential, MS-T(C), [11] was used to calculate the rate constants and estimate the effect of the different conformers of the reactants and saddle point, which was missed in previous studies. The term "conformers" refers to distinguishable structures that can be converted into each other by internal rotations.

Under the MS-T(C) scheme, the conformational rovibrational partition function is calculated as

$$Q_{con-rovib}^{MS-T(C)} = \sum_{j=1}^{J} Q_{rot,j} exp(-\beta U_j) Q_j^{HO} \prod_{\eta=1}^{t} \bar{f}_{j,\eta} \quad (1)$$

The set of conformers of each species (reactant or saddle point) is labeled as *J*. The conformer with the lowest potential energy (global minimum) is labeled as *j=1*, and the potential energy of each conformer, $U_j$, is defined with respect to that of the global minimum; therefore, $U_{j=1}$= 0. $Q_{rot,j}$ is the classical rotational partition function, the factor $\beta$ is $1/k_bT$ and $k_b$ is the Boltzmann's constant. The normal-mode harmonic oscillator partition function, $Q_j^{HO}$, is given by

$$Q_j^{HO} = \exp(-h\omega/2k_bT)[1 - \exp(-h\omega/k_bT)]^{-1} \quad (2)$$

and it is adjusted to account for the torsional anharmonicity associated to the coupled torsion $\eta$ by the term $\bar{f}_{j,\eta}$. In Eq. (2), $h$, $\omega$, and $T$ are the Planck's constant, frequency and temperature, respectively.

The product term of Eq. (1) is defined as

$$\prod_{\eta=1}^{t}\bar{f}_{j,\eta}=(2\pi\hbar\beta)^{t/2}\frac{\prod_{m=1}^{F}\omega_{j,m}}{\prod_{\bar{m}=1}^{F-t}\bar{\bar{\omega}}_{j,\bar{m}}}\frac{\sqrt{det\boldsymbol{D}_j}}{\prod_{\tau=1}^{t}M_{j,\tau}}\prod_{\eta=1}^{t}\exp\left(-\frac{\beta W_{j,\eta}^{(C)}}{2}\right)I_0\left(\frac{\beta W_{j,\eta}^{(C)}}{2}\right) \quad (3)$$

where $\bar{\bar{\omega}}_{j,\bar{m}}$ and $\boldsymbol{D}_j$ are the torsion-projected normal mode frequencies and the Kilpatrick and Pitzer torsional moment of inertia matrices, respectively. $M_{j,\tau}$ are the local periodicity parameters for uncoupled torsions $\tau$, and $I_0$ is a modified Bessel function.

Mutlti-structural torsional anharmonicity can be introduced by defining the multi-structural torsional anharmonicity factor $F_X^{MS-T(C)}$, where *X* stands for reactants, $F_R^{MS-T(C)}$, or saddle point, $F_{SP}^{MS-T(C)}$

$$F_X^{MS-T(C)}=Q_{con-rovib,X}^{MS-T(C)}/Q_{con-rovib,X,j=1}^{SS-T(C)} \quad (4)$$

$Q_{con-rovib,X,j=1}^{SS-T(C)}$ is the single-structural rovibrational partition function for the global minimum conformer of the species *X*, including torsional anharmonicity and coupled torsion, and is given by

$$Q_{con-rovib,j}^{SS-T(C)}=Q_{rot,j}exp(-\beta U_j)Q_j^{HO}\prod_{\eta=1}^{t}\bar{f}_{j,\eta} \quad (5)$$

The multi-structural torsional anharmonicity factor for the reaction can be calculated by using those for the reactants and saddle point (Eq. (4)) as

$$F^{MS-T(C)}=F_{SP}^{MS-T(C)}/F_R^{MS-T(C)} \quad (6)$$

Quantum effects on the reaction coordinate were included with the small-curvature tunneling approach (SCT),[12] obtaining the transmission coefficients $\kappa^{SCT}$. This approach considers the curvature of the reaction path and yields more accurate results than the Eckart approximation used in previous works.[5,6]

The final rate constant has been calculated as

$$k^{MS-T(C)/SCT}=\kappa^{SCT}\Gamma\frac{k_bT}{h}\frac{Q_{elec}^{\neq}Q_{con-rovib}^{MS-T(C),\neq}}{\Phi_tQ_{elec}^{R}Q_{con-rovib}^{MS-T(C),R}}\exp(-\beta V^{\neq}) \quad (7)$$

where the superscripts $\neq$ and *R* stand for conventional transition state and reactants, respectively, and $V^{\neq}$ is the classical barrier height defined with the global minimum conformers. The factor Γ is the recrossing transmission coefficient, given by the ratio of the CVT rate constant to the TST

one; CVT and TST stand for canonical variational and transition state theories, respectively. The relative translational and electronic partition functions are denoted as $\Phi_t$ and $Q_{elec}^{R}/Q_{elec}^{\neq}$, respectively. The terms $\kappa^{SCT}$ and Γ are also calculated using the global minimum structures and the harmonic oscillator approach.

Our kinetic study was based on electronic structure calculations at the CCSD(T)/aug-cc-pVYZ//M06-2X/cc-pVTZ *ab initio* level[13,14] (Y = T and Q for the reactions R1/R2 and R3, respectively); we used scaled vibrational frequencies by a factor of 0.955[15] in order to improve the description of the torsional anharmonicity as well as to obtain a more accurate adiabatic (ZPE-corrected, 0 K) potential energy curve. The electronic structure and minimum energy path calculations were performed with the software Gaussian09[16] and Gaussrate-2016,[17] respectively. The rate constants were calculated with the Polyrate-2016 code,[12] and the multi-structural partition functions were obtained with MSTor by using the Kilpatrick and Pitzer algorithm to calculate the moments of inertia.[18]

We used internal coordinates for the description of the normal modes perpendicular to the reaction coordinate. This led to a correct description of the reaction valley, with no imaginary frequencies along the MEP, and therefore to the correct adiabatic potential energy curve.

In order to assess the implications of our calculated rate constants in combustion, we performed kinetic model simulations using the ANSYS CHEMKIN-PRO 18.1 software.[19] We ran jet-stirred reactor (JSR) simulations for the oxidation of *sec*-, *n*- and *iso*-butanol isomers (s-$C_4H_9OH$, n-$C_4H_9OH$ and i-$C_4H_9OH$, respectively) with initial fuel mole fractions of 0.1% (0.001 fuel:0.006 $O_2$:0.993 $N_2$) at 10 atm and 850 K, and a residence time of 0.7 s. Closed batch reactor simulations for an stoichiometric mixture s-$C_4H_9OH$:air at 700 K and 1.9 atm were also run.

## 3. RESULTS AND DISCUSSION

### 3.1 Characterization of the potential energy surface

Figure 1 shows the adiabatic potential energy profile of the studied reactions at the CCSD(T)/aug-cc-pVYZ//M06-2X/cc-pVTZ level of theory (Y = T/Q). Only the global minimum structures of the species are shown; however, two different conformers were found for i-$C_3H_5OH$, $CH_2CHOH$ and HCOOH. The reactant 1-propenol shows two stereoisomers, (Z)-$CH_3CHCHOH$ and (E)-$CH_3CHCHOH$, each one with two different conformers; the former, whose global minimum is

0.23 kcal mol$^{-1}$ more stable than that of the latter, is shown in Figure 1. The saddle point species have a non-superimposable mirror image equivalent in energy. All these conformers were included in our kinetic study.

For the calculation of the periodicity parameters $M_{j,\tau}$, which are necessary to evaluate the multi-structural rovibrational partition functions (Eq. (1)) and thus the multi-structural anharmonicity factors (Eq. (4)), we used the schemes NS:SC = 3:0, 3:0, 3:0, 1:0, 2:0, 1:0, 1:0 and 1:0 for the species i-$C_3H_5OH$, (Z)-$CH_3CHCHOH$, (E)-$CH_3CHCHOH$, HCOOH, $CH_2CHOH$ and saddle points of the tautomerization of i-$C_3H_5OH$, (Z)-$CH_3CHCHOH$ and (E)-$CH_3CHCHOH$, respectively, where NS and SC respectively mean nearly separable and strongly coupled.

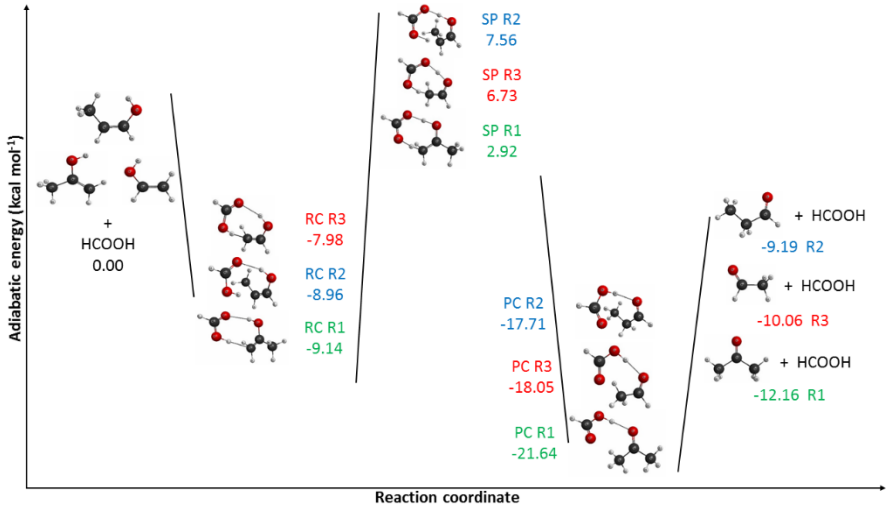


**FIGURE 1.** CCSD(T)/aug-cc-pV$Y$Z//M06-2X/cc-pVTZ adiabatic potential energy profile of the reactions R1/R2 ($Y$ = T, green/blue font) and R3 ($Y$ = Q, red font), defined with respect to the energy of the reactants. RC, PC and SP stand for reactant complex, product complex and saddle point, respectively.

### 3.2 Rate constants and transmission coefficients calculations

Figure 2 presents our calculated multi-structural torsional variational rate constants with SCT corrections ($\kappa^{SCT}$), $k^{MS-T(C)/SCT}$; these values are also tabulated in Table 1. Those calculated by Peeters[6] and da Silva[5] for the reaction R3 are also plotted for comparison. Our rate constants for the reaction R3 are significantly smaller than those calculated by da Silva, but larger than the ones

reported by Peeters. The reason for the high values of da Silva's rate constants is not clear; the lower adiabatic barrier of 6.6 kcal $mol^{-1}$ reported by da Silva compared to the values obtained by Peeters and us, 7.3 and 6.8 kcal $mol^{-1}$, respectively, as well as the use of the different methodology RRKM master equation, does not explain such large discrepancies. We infer that the discrepancies between our rate constants and Peeters's are mainly due to the different tunneling approaches used for the calculations. The Eckart approach used by Peeters and da Silva neglects the curvature of the reaction path, as opposed to the SCT method used in this work. At 298 K, the transmission coefficients yielded by these two approaches are $\kappa^{Eckart}$ = 17.7 and $\kappa^{SCT}$ = 193.3, proving the need for revisiting the reaction R3. It should be noted that da Silva[5] found that reaction R3 is pressure insensitive within the pressure range 0.01–100 atm, as expected for a $A + B \rightarrow C + D$ mechanism without bounded intermediates.

Multi-structural anharmonicity is also expected to be a source of discrepancy between our calculated rate constants and those by da Silva and Peeters. However, given the low number of conformers and mirror images of the studied stationary points, we do not expect this effect to be very large. For the three studied reactions, multi-structural anharmonicity factors vary from 2 at 100 K to 1 at 3000 K, and thus do not exert significant differences. They are included in our kinetic calculations in order to achieve high accuracy in the calculated rate constants, as well as to understand the reactivity at a more fundamental level.

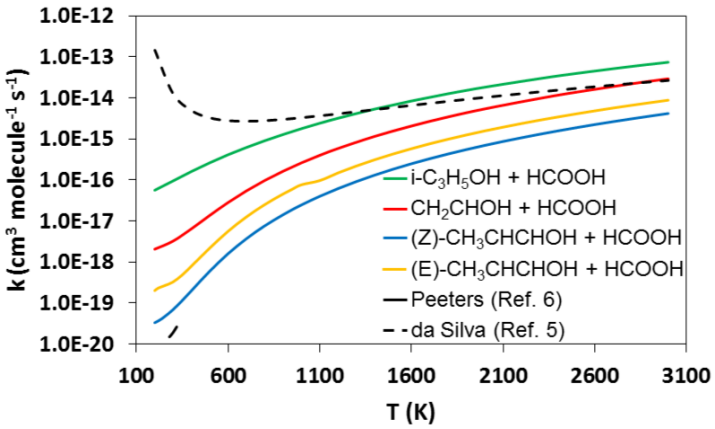


**FIGURE 2.** Plots of $k^{MS-T(C)/SCT}$ *versus* temperature for the reactions R1, R2(Z), R2(E) and R3 (green, blue, orange and red line, respectively). Results by Peeters (280–320 K) and da Silva for the reaction R3 are also plotted.

Enols with the OH group located on a terminal carbon atom, such as $CH_3CHCHOH$ and $CH_2CHOH$, cannot be expected to react similarly to those with the OH group located on a central carbon atom, like i-$C_3H_5OH$. The most reactive enol towards the HCOOH-catalyzed tautomerization is i-$C_3H_5OH$, followed by $CH_2CHOH$; $CH_3CHCHOH$ is the least reactive, and both stereoisomers, Z and E, show different reactivity besides their similar stability (our calculated standard enthalpies of formation are $\Delta H^o_{f,Z/E}$= -37.97/-37.87 kcal mol$^{-1}$). The reaction forming a ketone (R1) is faster than those producing an aldehyde (R2 and R3), as the former goes through a more stable saddle point; R1 is also more thermodynamically favored than R2 and R3. By comparing the saddle points of the reactions R2 and R3, both yielding an aldehyde, we infer that the additional methyl group attached to the double bond of $CH_3CHCHOH$ induces steric effects which contribute to making the corresponding saddle point more unstable, making the reaction slower. Steric effects might be also the reason for the lower stability of the transition state formed by (Z)-$CH_3CHCHOH$, with smaller rate constants than the reaction of (E)-$CH_3CHCHOH$.

The calculated rate constants shown in Table 1 were fitted to the following three-parameter two-term Arrhenius expression (in cm$^3$ molecule$^{-1}$ s$^{-1}$) in order to perform the simulations with CHEMKIN-PRO

$$k = A_1 \cdot T^{n_1} \exp\left(-\frac{E_{a,1}}{RT}\right) + A_2 \cdot T^{n_2} \exp\left(-\frac{E_{a,2}}{RT}\right) \qquad (8)$$

where $R$ and $T$ are the ideal gas constant and temperature with units of cal mol$^{-1}$ K$^{-1}$ and K, respectively. The fitting parameters $A_1$, $n_1$, $E_{a,1}$, $A_2$, $n_2$ and $E_{a,2}$ are tabulated in Table 2.

**TABLE 1.** Values of $k^{MS-T(C)/SCT}$ (cm$^3$ molecule$^{-1}$ s$^{-1}$) and $\kappa^{SCT}$ (unitless) for the reactions R1, R2 and R3.

| T (K) | $k_{R1}^{MS-T(C)/SCT}$ | $k_{R2,Z}^{MS-T(C)/SCT}$ | $k_{R2,E}^{MS-T(C)/SCT}$ | $k_{R3}^{MS-T(C)/SCT}$ | $\kappa_{R1}^{SCT}$ | $\kappa_{R2,Z}^{SCT}$ | $\kappa_{R2,E}^{SCT}$ | $\kappa_{R3}^{SCT}$ |
|---|---|---|---|---|---|---|---|---|
| 200 | $5.64\cdot10^{-17}$ | $3.32\cdot10^{-20}$ | $2.34\cdot10^{-19}$ | $2.07\cdot10^{-18}$ | $1.24\cdot10^{2}$ | $3.54\cdot10^{4}$ | $1.90\cdot10^{4}$ | $3.34\cdot10^{4}$ |
| 298 | $9.42\cdot10^{-17}$ | $6.82\cdot10^{-20}$ | $4.85\cdot10^{-19}$ | $3.21\cdot10^{-18}$ | $1.37\cdot10^{1}$ | $1.37\cdot10^{2}$ | $1.06\cdot10^{2}$ | $1.93\cdot10^{2}$ |
| 400 | $1.62\cdot10^{-16}$ | $2.00\cdot10^{-19}$ | $1.33\cdot10^{-18}$ | $6.47\cdot10^{-18}$ | 4.94 | $1.30\cdot10^{1}$ | $1.17\cdot10^{1}$ | $1.87\cdot10^{1}$ |
| 500 | $2.64\cdot10^{-16}$ | $6.00\cdot10^{-19}$ | $3.57\cdot10^{-18}$ | $1.38\cdot10^{-17}$ | 2.93 | 4.64 | 4.45 | 6.17 |
| 600 | $4.13\cdot10^{-16}$ | $1.60\cdot10^{-18}$ | $8.56\cdot10^{-18}$ | $2.83\cdot10^{-17}$ | 2.16 | 2.77 | 2.71 | 3.41 |

| | | | | | | | | |
|---|---|---|---|---|---|---|---|---|
| 800 | $9.10\cdot10^{-16}$ | $7.65\cdot10^{-18}$ | $3.43\cdot10^{-17}$ | $9.77\cdot10^{-17}$ | 1.56 | 1.73 | 1.71 | 1.94 |
| 1000 | $1.79\cdot10^{-15}$ | $2.47\cdot10^{-17}$ | $9.71\cdot10^{-17}$ | $2.62\cdot10^{-16}$ | 1.34 | 1.41 | 1.40 | 1.51 |
| 1200 | $3.21\cdot10^{-15}$ | $6.21\cdot10^{-17}$ | $2.20\cdot10^{-16}$ | $5.89\cdot10^{-16}$ | 1.23 | 1.26 | 1.26 | 1.33 |
| 1400 | $5.37\cdot10^{-15}$ | $1.32\cdot10^{-16}$ | $4.32\cdot10^{-16}$ | $1.16\cdot10^{-15}$ | 1.16 | 1.19 | 1.18 | 1.23 |
| 1600 | $8.47\cdot10^{-15}$ | $2.49\cdot10^{-16}$ | $7.66\cdot10^{-16}$ | $2.08\cdot10^{-15}$ | 1.12 | 1.14 | 1.14 | 1.17 |
| 1800 | $1.27\cdot10^{-14}$ | $4.32\cdot10^{-16}$ | $1.26\cdot10^{-15}$ | $3.46\cdot10^{-15}$ | 1.10 | 1.11 | 1.11 | 1.13 |
| 2000 | $1.83\cdot10^{-14}$ | $7.00\cdot10^{-16}$ | $1.95\cdot10^{-15}$ | $5.42\cdot10^{-15}$ | 1.08 | 1.09 | 1.09 | 1.11 |
| 2300 | $2.98\cdot10^{-14}$ | $1.31\cdot10^{-15}$ | $3.46\cdot10^{-15}$ | $9.79\cdot10^{-15}$ | 1.06 | 1.06 | 1.06 | 1.08 |
| 2500 | $3.98\cdot10^{-14}$ | $1.90\cdot10^{-15}$ | $4.86\cdot10^{-15}$ | $1.39\cdot10^{-14}$ | 1.05 | 1.05 | 1.05 | 1.07 |
| 3000 | $7.46\cdot10^{-14}$ | $4.19\cdot10^{-15}$ | $1.01\cdot10^{-14}$ | $2.95\cdot10^{-14}$ | 1.03 | 1.04 | 1.04 | 1.05 |

**TABLE 2.** Values of the fitting parameters $A$ (cm$^3$ molecule$^{-1}$ s$^{-1}$), $n$ (unitless) and $E_a$ (cal mol$^{-1}$) of Eq. (8) for the studied reactions.

| Reaction | $A_1$ | $n_1$ | $E_{a,1}$ | $A_2$ | $n_2$ | $E_{a,2}$ |
|---|---|---|---|---|---|---|
| R1 | $1.000\cdot10^{-1}$ | 3.240 | -1000 | $8.00\cdot10^{-3}$ | 3.600 | 1000 |
| R2/Z | $1.271\cdot10^{-4}$ | 3.880 | 2761 | $2.353\cdot10^{-6}$ | 3.800 | 1079 |
| R2/E | $2.285\cdot10^{-3}$ | 3.671 | 2148 | $4.434\cdot10^{-3}$ | 2.902 | 748 |
| R3 | $3.000\cdot10^{-3}$ | 3.400 | -650 | $9.000\cdot10^{-3}$ | 3.600 | 3500 |

To cast light on the large values of $\kappa^{SCT}$ we looked into the SCT tunneling probability at a given energy, which is defined as

$$P_{SCT}(E) = \left[1 + exp\left(\frac{2}{\hbar}\int_{s-}^{s+}\sqrt{2\mu(s)_{eff}[V_a^G(s) - E]}\,ds\right)\right]^{-1} \quad (9)$$

where $\hbar$ is the Planck's constant divided by 2π, $\mu(s)_{eff}$ is the effective reduced mass as function of the reaction coordinate $s$, which includes the reaction path curvature, $V_a^G(s)$ is the ground-state adiabatic potential energy, and $s-$ and $s+$ are turning points where $V_a^G(s) = E$ on the left and right sides of the maximum of the $V_a^G(s)$ curve, respectively. $P_{SCT}(E)$ was calculated at energies ranging from the sum of the ZPE of the reactants up to the maximum of the $V_a^G(s)$ curve, called $V_a^{G,max}$, and $P_{SCT}(E)$ reaches a maximum value of 0.5; $\kappa^{SCT}(T)$ is calculated as

$$\kappa^{SCT}(T) = \frac{1}{RT}\int_{E_o}^{+\infty} P_{SCT}(E)exp\left[-\left(E - V_a^{G,max}\right)/RT\right]dE \quad (10)$$

where R is the ideal gas constant. The adiabatic potential energy curve and the values of the integrand of Eq. (10) at 200 K as function of the energy $E$ are represented in Figures 3(a) and 3(b), respectively, for the investigated reactions. Those for the $HO_2$-catalyzed tautomerization of i-$C_3H_5OH$ recently investigated by us[7] are also plotted for comparison purposes. The values of $E$ used to define the x-axis of Figure 3(b) are defined with respect to the value of $V_a^{G,max}$, so that $E = 0.0$ kcal mol$^{-1}$ represents the top of the $V_a^G(s)$ barrier and the lowest energy value $E_o$ represents the lower energy limit for the calculations of $\kappa^{SCT}(T)$.

A different approach could be used to calculate the transmission coefficients in which the lower energy limit for the calculations is set to the ZPE of the intermediate reactant complex. These intermediate complexes can be collisionally stabilized in the high pressure limit and may enhance tunneling by promoting this effect at lower energies than that of the reactants. However, we do not expect this approach to yield different values of $\kappa^{SCT}$ unless much lower temperatures are reached. We used these two approaches in our recent work[7] and demonstrated that both yield essentially the same $\kappa^{SCT}$ values within the temperature range 200–3000 K. However, at temperatures below 200 K significant differences were observed.

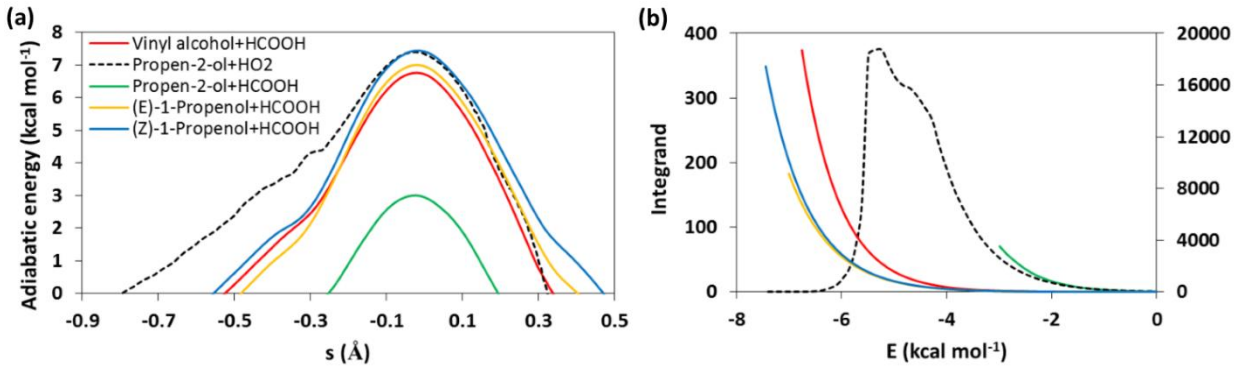


**FIGURE 3.** Plots of the adiabatic potential energy curves (a) and values of the integrand of Eq. (10) at 200 K (b) for the reactions R1, R2(Z), R2(E) and R3 (green, blue, orange and red line, respectively). Blue, orange and red lines in panel (b) are represented by the secondary axis. The curves of the $HO_2$-catalzyed tautomerization of propen-2-ol previously studied by us[7] are also represented for comparison (dashed black line).

Reaction R1, with the lowest barrier, shows the smallest tunneling coefficients; reactions R2/Z, R2/E and R3 show a more pronounced tunneling effect (Table 1). The most interesting behavior of the curves of the HCOOH-catalyzed reactions in Figure 3(a) is the sudden drop in the area near the saddle point, which induces a very narrow adiabatic curve; this is not the case of the $HO_2$-catalyzed reaction. This has important implications in the values of $\kappa^{SCT}(T)$, as narrow adiabatic energy curves yield large values of tunneling probabilities (Eq. (9)) and consequently large tunneling coefficients (Eq. (10)). This is exemplified by the variation of the integrand of Eq. (10) as function of energy shown in Figure 3(b), from which can be concluded that the system in the HCOOH-catalyzed reactions can tunnel even at energies equal to $E_o$. The $HO_2$-catalyzed tautomerization shows values of zero for that integrand at energies equal to $E_o$, which only rises at higher energies when the adiabatic energy curve is narrow enough. In addition, the larger and more flexible structure of the catalyzer HCOOH than that of the $HO_2$ might help to form a less tight saddle point for the double hydrogen shift reaction, inducing a lower barrier height, 2.92 and 7.25[7] kcal mol$^{-1}$, respectively.

HCOOH seems to catalyze effectively double hydrogen shift reactions,[20] and may represent a larger sink of enols than $HO_2$ in the atmosphere and in combustion. This is especially important in the atmosphere, where the concentration of HCOOH is of the order of $1 \cdot 10^{11}$ molecules cm$^{-3}$,[21] while that of the $HO_2$ radical is approximately two orders of magnitude lower,[22] and tunneling plays a role. For instance, the standard free energy barriers to the HCOOH-catalyzed, $HO_2$-catalyzed and non-catalyzed tautomerizations of i-$C_3H_5OH$ are 14.26, 17.91 and 53.64 kcal mol$^{-1}$, respectively.

One should be cautious when establishing analogies in kinetic modeling, especially at low temperatures when the rate constants are more sensitive to the barrier height and tunneling effect. $C_3$ and larger enols have been demonstrated to exist in hydrocarbon and commercial fuel flames,[1] supporting their inclusion in flame models. Our calculated rate constants are useful to establish more accurate analogies to describe those enols than that of the vinyl alcohol,[5] facilitating the kinetic modelling of certain fuels. For instance, we suggest that the HCOOH-catalyzed tautomerizations of 1-buten-2-ol and 2-buten-2-ol may be modelled by our calculated rate constants for the reaction R1, as these enols have a non-terminal OH group (yielding a ketone) and alkyl groups attached to the double bond, while those of 1-buten-1-ol, 1-penten-1-ol and 3,3-

dimethyl-1-penten-1-ol may be modelled by the calculated rate constants for the reaction R2 since these enols have a terminal OH group (yielding an aldehyde) as well as alkyl groups attached to the double bond.

### 3.3 Kinetic modelling

Finally, we show the effect of the calculated rate constants for the reactions R1, R2(Z) and R3 in the combustion of the s-$C_4H_9OH$, n-$C_4H_9OH$ and i-$C_4H_9OH$ butanol isomers. We updated the former kinetic model for butanol[7] with our calculated rates and the abovementioned analogies, and obtained an updated model. We ran jet-stirred reactor (JSR) simulations for the oxidation of s-$C_4H_9OH$, n-$C_4H_9OH$ and i-$C_4H_9OH$ with initial fuel mole fractions of 0.1% (0.001 fuel:0.006 $O_2$:0.993 $N_2$) at 10 atm and 850 K, and a residence time of 0.7 s, using the ANSYS CHEMKIN-PRO 18.1 software.[19] Figure 4 shows the steady concentrations of acetaldehyde and vinyl alcohol in the JSR simulations for the three butanol isomers.

Compared to the concentrations predicted by the former model for acetaldehyde and vinyl alcohol (Figure 33 of Ref. [8]), we conclude that the updated model predicts a higher concentration of vinyl alcohol and lower concentration of acetaldehyde. For the isomers n-$C_4H_9OH$, s-$C_4H_9OH$ and i-$C_4H_9OH$, the updated model predicts a concentration of vinyl alcohol which is respectively 2.7, 2.3 and 1.1 times larger than that predicted by the former model. This might be due to the overestimation of the rate constants made by da Silva for the reaction R3.[5] With our calculated rate constants the reaction R3 is not as important as a sink of vinyl alcohol, and therefore we predict a larger amount of vinyl alcohol which, under certain conditions, may be prone to further oxidation to produce HCOOH. This may help to provide the necessary budget of atmospheric vinyl alcohol (and other enols, based on our new analogue reactions) to explain why current atmospheric kinetic models underestimate the concentration of carboxylic acids by a factor of $\approx 2$.[23] Given the numerous possible sources and sinks for enols in the atmosphere, this conclusion remains to be proved by detailed atmospheric modelling. The present kinetic study is useful for this purpose.

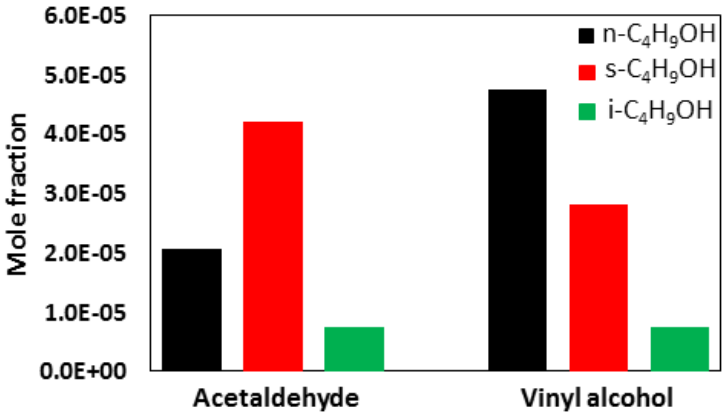


**FIGURE 4.** Steady concentrations of acetaldehyde and vinyl alcohol in the JSR simulations with 0.001 fuel:0.006 $O_2$:0.993 $N_2$ mixtures of s-$C_4H_9OH$, n-$C_4H_9OH$ and i-$C_4H_9OH$ at 10 atm and 850 K.

The results of the closed batch reactor simulations of an stoichiometric mixture s-$C_4H_9OH$:air at 700 K and 1.9 atm with both models are shown in Figure 5. The former model overestimated the role of the reactions R1, R2 and R3 and consequently, the species concentration profiles of the corresponding reactants and products are affected when the kinetic model is updated. With the former model, the reaction R1 is prominent in the consumption of i-$C_3H_5OH$ and production of $CH_3COCH_3$; that is not the case with the updated model, and the reaction R1 becomes less prominent and competes with the unimolecular tautomerization. Similarly, the reaction R3 becomes less important in the production of $CH_3CHO$ with the updated model.

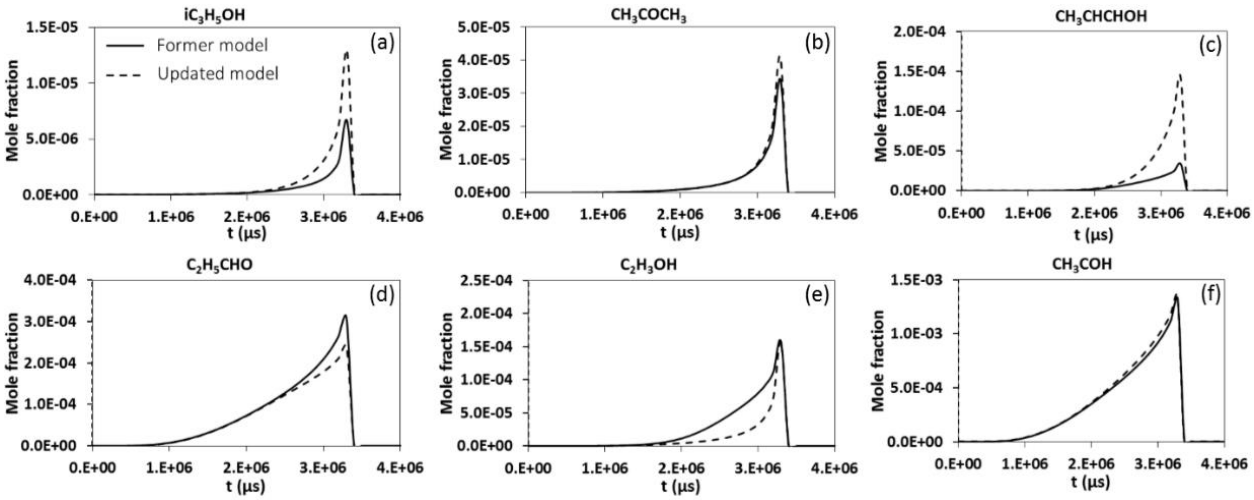


**FIGURE 5.** Species concentration profiles for propen-2-ol (a), acetone (b), 1-propenol (c), propanal (d), vinyl alcohol (e) and acetaldehyde (f) in the combustion of a stoichiometric mixture s-$C_4H_9OH$:air at 1.9 atm and 700 K using the former and updated models in a closed batch reactor.

## 4. CONCLUSION

This work demonstrates the need for calculating the rate constants for the formic acid catalyzed keto–enol tautomerizations converting propen-2-ol and 1-propenol into acetaldehyde and acetone, respectively, as well as revisiting those for the formic acid catalyzed keto–enol tautomerization converting vinyl alcohol into acetaldehyde. Our calculated rate constants are based on high level electronic structure calculations at the CCSD(T)/aug-cc-pVYZ//M06-2X/cc-pVTZ level of theory (X = T/Q), and include further improvements such as multi-structural torsional anharmonicity and curvature in the tunneling coefficients, which were missed in previous studies.

The studied double hydrogen shift reactions show narrow adiabatic potential energy curves, and therefore enhance a tunneling mediated mechanism at low temperatures which turned out to be very important and yielded much larger tunneling coefficients than the Eckart approach used in former studies.

This study also provides new and more accurate analogies for kinetic modeling of larger enols and aldehydes/ketones, and predicts that formic acid is a very efficient catalyzer of the keto–enol tautomerization.

We prove that former kinetic models in combustion may overestimate the role of the formic acid catalyzed keto–enol tautomerization of vinyl alcohol as sink of that enol. Our work may help to improve the predictions on the concentration of tropospheric carboxylic acids, which is currently underestimated in atmospheric models, by providing accurate rate constants for the keto–enol tautomerizations of $C_2$ and $C_3$ enols.


## ACKNOWLEDGMENTS

We acknowledge funding from King Abdullah University of Science and Technology (KAUST), Office of Sponsored Research (OSR), Award No. OSR-2016-CRG5-3022 and the resources of the Supercomputing Laboratory at KAUST. We are grateful to Maria Cecilia Alvarado Bernaldez for her assistance in designing and elaborating the TOC graphic.



## ORCID

M. Monge-Palacios: 0000-0003-1199-5026

E. Grajales-González: 0000-0002-2317-0884

S. Mani Sarathy: 0000-0002-3975-6206


## REFERENCES


[1] C. A. Taatjes, N. Hansen, A. Mcllroy, J. A. Miller, J. P. Senosiain, S. J. Klippenstein, F. Qi, L. Sheng, Y. Zhang, T. A. Cool *et al*., *Science* **2005**, 308, 1887-1889.

[2] D. U. Andrews, B. R. Heazlewood, A. T. Maccarone, T. Conroy, R. J. Payne, M. J. T. Jordan, S. H. Kable, *Science* **2012**, 337, 1203-1206.

[3] M. F. Shaw, B. Sztaray, L. K. Whalley, D. E. Heard, D. B. Millet, M. J. T. Jordan, D. L. Osborn, S. H. Kable, *Nature. Comm.* **2018**, 9, 2584.

[4] E. Grajales-González, M. Monge-Palacios, S. Mani Sarathy, *J. Phys. Chem. A* **2018**, 122, 3547-3555.

[5] G. da Silva, *Angew. Chem. Int. Ed.* **2010**, 49, 7523-7525.

[6] J. Peeters, V. S. Nguyen, J-F Muller, *J. Phys. Chem. Lett.* **2015**, 6, 4005-4011.

[7] M. Monge-Palacios, E. Grajales-González, S. Mani Sarathy, *J. Phys. Chem. A* **2018**, 122, 9792-9805.

[8] S. Mani Sarathy, S. Vranckx, K. Yasunaga, M. Mehl, P. Oßwal, W. K. Metcalfe, C. K. Westbrook, W. J. Pitz, K. Kohse-Hoinghaus, K. Fernandes *et al*., *Combust. Flame* **2012**, 159, 2028-2055.

[9] L. A. Curtiss, P. C. Redfern, K. Raghavachari, J. A. Pople, *J. Chem. Phys*. **2001**, 114, 108-117.

[10] S. Mani Sarathy, P. Oßwald, N. Hansen, K. Kohse-Höinghaus, *Energy Combust. Sci*. **2014**, 44, 40-102.

[11] J. Zheng, D. G. Truhlar, *J. Chem. Theory Comput*. **2013**, 9, 1356-1367.

[12] J. Zheng, J. L. Bao, R. Meana-Pañeda, S. Zhang, B. J. Lynch, J. C. Corchado, Y-Y Chuang, P. L. Fast, W-P. Hu, Y-P Liu *et al*. POLYRATE-version 2016-2A, University of Minnesota: Minneapolis **2016**.

[13] Y. Zhao, D. G. Truhlar, *Theor. Chem. Acc*. **2008**, 120, 215-241.

[14] R. J. Bartlett, *J. Phys. Chem*. **1989**, 93, 1697-1708.

[15] NIST Computational Chemistry Comparison and Benchmark Database, NIST Standard Reference Database Number 101 2016, Ed. Russell D. Johnson III.

[16] M. J. Frisch, G. W. Trucks, H. B. Schlegel, G. E. Scuseria, M. A. Robb, J. R. Cheeseman, G. Scalmani, V. Barone, B. Mennucci, G. A. Petersson *et al*., Gaussian 09, Gaussian, Inc, Wallingford, CT **2010**.

[17] J. Zheng, S. Zhang, J. C. Corchado, R. Meana-Pañeda, Y. Y. Chuang, E. L. Coitiño, B. A. Ellingson, D. G. Truhlar, GAUSSRATE 2016, University of Minnesota: Minneapolis **2016**.

[18] J. Zheng, S. L. Mielke, J. L. Bao, R. Meana-Pañeda, K. L. Clarkson, D. G. Truhlar, MSTor, version 2017-B, University of Minnesota: Minneapolis **2017**.

[19] Reactor Design, CHEMKIN-PRO18.1: San Diego **2017**.

[20] M. Monge-Palacios, M. P. Rissanen, Z. Wang, S. Mani Sarathy *Phys. Chem. Chem. Phys*. **2018**, 20, 10806-10814.

[21] Z. Meng, J. H. Seinfeld, *Aerosol Science and Technology* **1995**, 23, 561-578.

[22] F. Holland, A. Hofzumahaus, J. Schafer, A. Kraus, H.-W. Patz, *J. Geophys. Res.* **2003**, 108, 1-21.

[23] A. E. Clubb, M. J. T. Jordan, S. H. Kable, D. L. Osborn, *J. Phys. Chem. Lett.* **2012**, 3, 3522-3526.